Density functional study of x-ray Raman scattering from aromatic hydrocarbons and polyfluorene

A. Sakko, M. Hakala, J. A. Soininen, and K. Hämäläinen
Division of x-ray Physics, Department of Physical Sciences, University of Helsinki, FIN-00014 Helsinki, Finland
(Received 3 May 2007; revised manuscript received 20 September 2007; published 26 November 2007)

We present a computational method for studying local electronic structure of molecular materials in the framework of nonresonant inelastic x-ray scattering from inner-shell excitations. Our method enables a detailed analysis of the experimental spectrum and thus provides insight into the density, orientation, and the symmetries of the unoccupied electronic states. The method employs transition potential approximation within the density functional theory. We report results for a set of aromatic molecules and for aligned poly[9,9-bis(2-ethylhexyl)-fluorene-2,7-diyl]. Our results are found to be in good agreement with the experimental data in the near-edge region.

DOI: 10.1103/PhysRevB.76.205115 PACS number(s): 71.20.Rv, 78.70.Ck, 33.20.Rm

I. INTRODUCTION

Molecular materials attract interest in many branches of science and technology. Polymers, liquid crystals, nanostructures, and many organic compounds already have numerous applications, and a wide variety of possibilities has been proposed for the future. When developing new materials with tailored properties, a detailed understanding of their electronic structure is essential. Many experimental methods for studying these properties are employed, including nonresonant inelastic x-ray scattering from inner-shell excitations, often called x-ray Raman scattering[1,2] (XRS). One of the specific and most advantageous features of XRS is that it allows the study of the localization and the symmetries of the unoccupied electronic states.[3,4] These properties are closely related to many important characteristics of the material, such as the atomic structure, chemical bonding, and optical as well as electrical properties. Solid state structures have been the primary focus of XRS studies in the past, but a very recent experimental work showed that XRS is suitable for studying organic polymers as well.[5] In this work we present a method for calculating XRS cross sections for molecular systems. The method facilitates a detailed analysis of the underlying electronic structure responsible for the features in XRS spectrum of molecular systems.

X-ray Raman spectroscopy was developed in the 1960s after the pioneering experimental work by Suzuki *et al.*[6] and the theoretical explanation by Mizuno and Ohmura.[7] They showed that using low scattering angles, x-ray Raman scattering probes the same dipole transitions as the x-ray absorption spectroscopy[8,9] (XAS) and thus provides the same information on the sample.[10] However, the experimental conditions for XRS and XAS can be very different. In XAS, the energy of the incoming photons must be near the binding energy of the inner-shell electron ($\lesssim$1 keV for light elements). In XRS the energy of the incoming photons is usually 8–12 keV, and the energy *transfer* from the photons to the system is near the binding energy. The higher energy of the photons leads to better penetration into the sample and decreased absorption in the environment, making XRS a true bulk probe applicable to extreme sample environments.[2] Furthermore, using high scattering angles in XRS allows the study of nondipole transitions as well.[10] XRS has traditionally been restricted to low-Z elements, but recently also heavier elements have been studied.[11] After the advent of the third generation synchrotron sources in the 1990s, the power of XRS has been realized in many branches of material sciences. XRS has been utilized to study chemical bonding,[12] core excitons,[13,14] phase transitions under high pressure,[15] and the symmetries of the unoccupied states.[3,4] The drawback of XRS is a low scattering cross section and a relatively weak energy resolution (typically $\sim$1 eV). The third method applicable for studying inner-shell excitations is the electron energy loss spectroscopy[16,17] (EELS). It is analogous to XRS, but the probing particles are electrons instead of x-ray photons. At high scattering angles, EELS can also be used to probe the nondipole transitions. Furthermore, the strong interaction of the electrons with the sample material, together with the high energy resolution and the applicability to high-Z elements makes EELS a substantial alternative, especially for the surface studies. However, the multiple scattering of the probe electrons in the sample material can lead to a demanding data analysis.[18] In XRS the interaction is much weaker and multiple scattering can be typically neglected in the analysis.

The diverse use of XRS is a consequence of the fact that the measured spectrum contains a wealth of information on electronic and structural properties of the sample. The extended region of the spectrum (i.e., when the energy transfer is more than a few tens of eVs above the studied edge) contains oscillations that can be associated with the structural properties of the sample, such as coordination numbers and bond lengths.[19,20] In contrast to this, the interpretation of the near-edge spectrum (often called XANES, x-ray absorption near-edge structure) is not as straightforward and usually needs the comparison with calculated spectrum. Various theoretical schemes have been employed to model the electronic transition from an inner-shell state to the unoccupied states. For solids, a recently developed approach, based on the Bethe-Salpeter equation and GW approximation, can be used.[21,22] Different methods are needed for molecules and other nonperiodic systems, and usually it is adequate to work at the level of Hartree-Fock[23] (HF) or density functional theory[24–26] (DFT). In these two approaches, the time-dependence of the system can be approximated by a static potential which includes the orbital relaxation effects of the electronic system. This scheme is utilized in many methods,

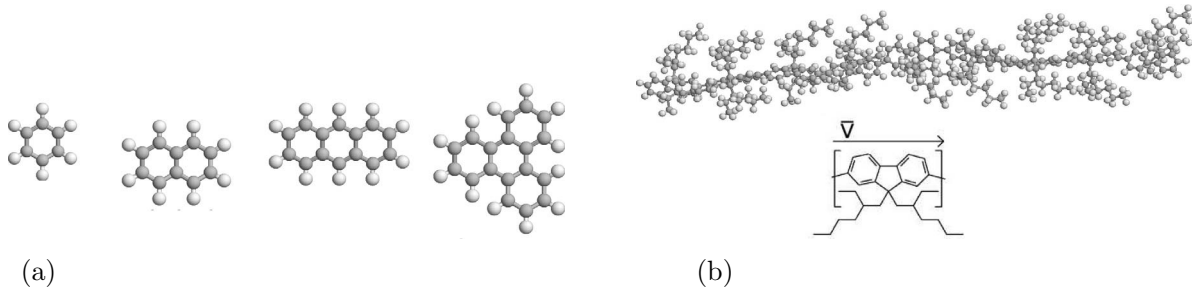

FIG. 1. Molecules and the polymer studied in this work. (a) From left: benzene, naphthalene, anthracene, and tripenylene. (b) The polymer chain and the structure of one monomer of polyfluorene PF6/2. For polyfluorene, only one monomer was included in the calculation. The consecutive monomers in polyfluorene are curled around the drawing axis of polymer (pointing towards **v**), and thus the direction of a single monomer is not exactly parallel to the drawing axis (Ref. 46).

such as the static exchange,[27] transition potential (TP) approximation,[28] and $Z+1$ approximation.[29] The advantage of these methods is their computational efficiency. However, also quite sophisticated computational schemes have been used.[30–32] In this work we concentrate on the TP approach within DFT. This is a TP-DFT based study of XRS with varying momentum transfer. A method with only dipole transitions has been applied to XAS by Triguero *et al.*[25] We also illustrate how the transition rates can be separated into different transition channels and thus study the symmetry properties of the unoccupied states.

The systems studied in this work are four aromatic hydrocarbon molecules and aligned polyfluorene. Aromatic hydrocarbons are the building blocks of various more complex and technologically important compounds.[33] Poly[9,9-bis(2-ethylhexyl)-fluorene-2,7-diyl] is a π-conjugated polymer that has interesting electrical and optical properties.[34–36] The very recent work of Galambosi *et al.*[5] showed for the first time that XRS can be applied for studying the electronic structure of such polymers.

II. THEORETICAL BACKGROUND

When a photon scatters inelastically from the sample, some amount of energy ω and momentum $\mathbf{q}$ is transferred to the scattering system.[37] If the energy of the incoming photon is far from the absorption edges of the sample material, the resonant inelastic x-ray scattering can be neglected. For the typical x-ray energies it is adequate to work within the nonrelativistic limit, and then the standard theoretical approach for XRS is to use the Fermi golden rule for the electronic transitions induced by the interaction of the electromagnetic field with the electrons.[1] The double differential cross section can be written as

$$\frac{d\sigma}{d\Omega d\omega} = \left(\frac{d\sigma}{d\Omega}\right)_{Th} S(\mathbf{q},\omega), \tag{1}$$

where $\left(\frac{d\sigma}{d\Omega}\right)_{Th}$ is the Thomson scattering cross section and $S(\mathbf{q},\omega)$ the dynamic structure factor. The energy transfer is $\omega=\omega_1-\omega_2$, where ω_1 and ω_2 are the energies of the incoming and outgoing photons, respectively. Similarly, the momentum transfer is $\mathbf{q}=\mathbf{q}_1-\mathbf{q}_2$, where $\mathbf{q}_1$ and $\mathbf{q}_2$ are the momenta of the incoming and outgoing photons, respectively. If the system is in the ground state before the scattering process, the dynamic structure factor is

$$S(\mathbf{q},\omega) = \sum_F \left| \left\langle I \left| \sum_n e^{i\mathbf{q}\cdot\mathbf{r}_n} \right| F \right\rangle \right|^2 \delta(\omega + E_I - E_F), \tag{2}$$

where the sum inside the brackets is taken over all the electrons in the scattering system. $|I\rangle$ is the initial state, i.e., the ground state, and $\{|F\rangle\}$ are the final states of the scattering system. E_I and E_F are the total energies of the initial and the final states, respectively.

Within Kohn-Sham DFT (KS-DFT), the occupied Kohn-Sham orbitals can be used to construct a Slater determinant which approximates the true wave function of the system.[38–40] The unoccupied KS orbitals can be considered as the final one-electron states of the excited electron. However, the electronic excitation created in the XRS process induces changes in the electronic structure. A considerable part of these relaxation effects, or core hole effects, can be included using TP approximation.[28] In this approach the occupancies of the initial and the final one-electron states are set to 0.5 in the self-consistent calculation, while the occupancies of the other states remain unchanged. The approximation was introduced in the framework of the $X\alpha$ method, and Janak's theorem justified the validity of the approximation within DFT as well.[41] TP-DFT has indeed provided good results for XAS.[25,42,43]

Using KS-DFT within TP approximation, the XRS contribution to the dynamic structure factor can be written as

$$S(\mathbf{q},\omega) \approx \sum_f |\langle i|e^{i\mathbf{q}\cdot\mathbf{r}}|f\rangle|^2 \delta(\omega + \varepsilon_i - \varepsilon_f). \tag{3}$$

Here $|i\rangle$ is the one-electron state related to the initial KS orbital and the sum is over all the unoccupied KS orbitals, i.e., final one-electron states $|f\rangle$. The distribution of the one-electron eigenvalues ε_n determines the density of states, and the XRS transition matrix elements $\langle i|e^{i\mathbf{q}\cdot\mathbf{r}}|f\rangle$ determine the transition rates between the initial and the final states. If small scattering angles are used in the experiments, the magnitude of the momentum transfer is small and all but the first terms of the expansion of the exponential in the transition matrix element can be neglected. Due to the orthogonality of the KS orbitals the matrix elements can then be approximated by the dipole matrix elements $\langle i|\mathbf{r}|f\rangle$, which determine

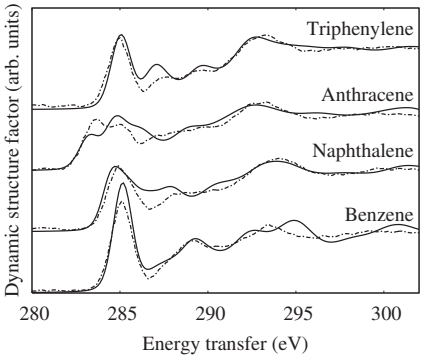

FIG. 2. Calculated (solid lines) and experimentally measured (Ref. 45) (dash-dotted lines) dynamic structure factors for the carbon K edge of unoriented aromatic hydrocarbons in the dipole region.

the so-called oscillator strengths and thus the absorption cross section. Using high scattering angles in XRS and EELS, the full exponential must be included and one probes also nondipole transitions.

III. RESULTS

The KS-DFT calculations performed in this work were carried out using an all-electron code STOBE-DEMON, where the possibility to use TP approximation has been implemented.[44] The code has been used also in the XAS calculations.[25] Because the program employs localized Gaussian type orbitals, the calculation of the transition matrix element reduces to a sum of integrals. Due to the properties of the Gaussian functions, these integrals have analytic solutions, which allows a fast and numerically stable calculation of $S(\mathbf{q},\omega)$. We will call this the Gaussian integral based method to distinguish it from another approach needed in the symmetry analysis of the final states and presented in Sec. III B.

A. Comparison with experiments

To illustrate the applicability of our method, we performed calculations for the carbon K edge of benzene, naphthalene, anthracene, triphenylene, and aligned polyfluorene. The systems are shown in Fig. 1, and their geometries are described in Refs. 45 and 46. The calculated spectra were compared with experimental results that are from Refs. 5 and 45. We varied the momentum transfer vector so that both the effects of its magnitude and direction on the spectrum were studied. Triple-ζ plus valence polarization type basis sets were used for all hydrogen and nonexcited carbon atoms. For the excited carbon site we used the iii-iglo basis set together with a set of diffuse basis functions.[47] They improve the description of the orbital relaxation effects and the modeling of the delocalized unoccupied states, as described in Ref. 25 and in references therein. Gradient-corrected exchange-correlation functional[48,49] was employed in the calculations. To create a well-localized core orbital, we used the model core potential method[50] (MCP). With MCP, the nucleus and the inner-shell electrons of all the carbon atoms except the excited one are replaced by model potentials. This ensures the localization of the initial carbon 1s orbital. In this work separate calculations were performed for all inequivalent carbon sites, and the final spectra were obtained as appropriately weighted averages of these calculations.

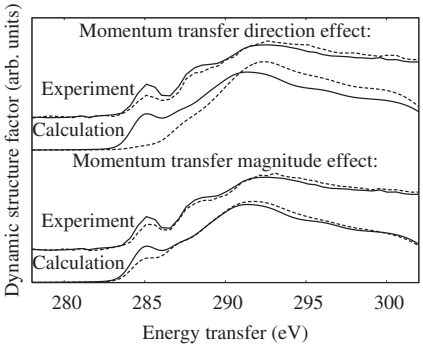

FIG. 3. Calculated and experimental (Ref. 5) dynamic structure factors for the carbon K edge of aligned polyfluorene with different momentum transfers. In the upper curves $\mathbf{q}$ is perpendicular to (solid line) or along (dashed line) the drawing axis of the polyfluorene, and its magnitude is 1.40 a.u. In the lower curves $\mathbf{q}$ is perpendicular to the drawing axis, and its magnitude is 1.40 a.u. (solid line) or 5.13 a.u. (dashed line).

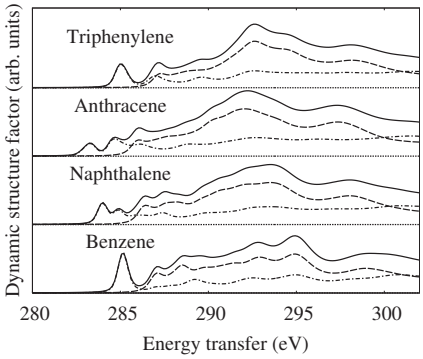

FIG. 4. Calculated dynamic structure factors for the carbon K edge of unoriented aromatic hydrocarbons in the nondipole region (q=9.0 a.u.), and the final state decomposition. Solid lines: total dynamic structure factor, dashed lines: s-type contribution, dash-dotted lines: p-type contribution, and dotted lines: d-type contribution (negligible).

Typically the absolute values for the absorption edge energies obtained from KS-DFT calculations are not exactly equal to the experimental ones. In this work a rigid energy shift ($\sim$2 eV) was implemented to the calculated spectra (Figs. 2–5) to align the main peaks with the experiments.[51] To facilitate the comparison with the experimental results, the areas under the curves in the figures were normalized to the same value in the energy range 280–302 eV. The calculated spectra were also broadened with energy-dependent Lorentzian and constant Gaussian line shapes. The former of these stands for the lifetime broadening and the latter for the instrumental broadening. The Lorentzian line shape is proportional to $\Gamma_\omega/(\omega^2+\Gamma_\omega^2/4)$, where Γ_ω is the full width at half maximum (FWHM). Relatively good estimates for the magnitude of the lifetime broadening can be calculated for solids,[9] but for molecules the FWHM is traditionally approximated by some simple function that gives a sufficient agreement between the linewidths of the calculated and the

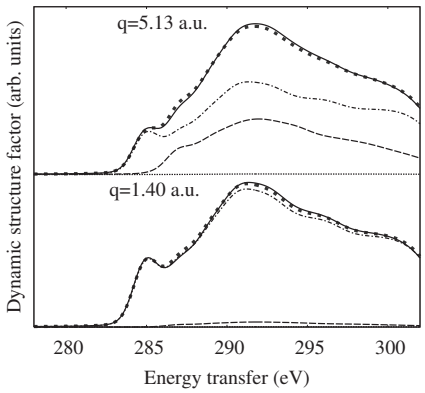

FIG. 5. Calculated dynamic structure factors and the final state decompositions for the carbon *K* edge of aligned polyfluorene for two different momentum transfers, both perpendicular to the drawing axis of the polyfluorene. Solid lines: total dynamic structure factor (calculated using the Gaussian integral based method), dashed lines: *s*-type contribution, dash-dotted lines: *p*-type contribution, dotted lines: *d*-type contribution (negligible), and squares: sum of *s*-, *p*-, and *d*-type contributions.

experimentally measured spectra. In this work we employed a linearly increasing function $\Gamma_\omega = 0.01\ \text{eV} + 0.17(\omega - 283\ \text{eV})$.

In Fig. 2 we present the calculated and the experimentally measured[45] spectra for the aromatic molecules in the low momentum transfer region. Since the samples in the experiments were unoriented, the calculations were done by averaging over the directions of the momentum transfer. The reported experimental energy resolution was 1.1 eV, and this value was also used in the Gaussian broadening procedure. All main features of the experimental spectra are reproduced by our calculations. For example, the four unequivalent carbon sites with slightly different 1*s* excitation energies in anthracene lead to a relatively broad peak at around 285 eV. This is in contrast to benzene, where all carbon sites are equivalent and the peak is narrow. This explanation is consistent with Gordon *et al.*[45] who used HF calculations. The discrepancies of the spectra in Fig. 2 are related mainly to the peak intensities, where slight variations between the calculated and the experimentally measured spectra can be seen. Furthermore, some of the peaks in the calculated spectra seem to be too sharp, which can be in part due to the very simple model we have used for the lifetime broadening.

When performing the calculations for the aligned polyfluorene, only one monomer (29 carbon atoms and 42 hydrogens) was included. Two orientations of the momentum transfer were studied: perpendicular and along the drawing axis of the polyfluorene. The polyfluorene is formed by consecutive monomers that are curled around the drawing axis. The angle between the backbone of the monomer and the drawing axis (see Fig. 1) was 16.5°, approximately corresponding to the often suggested five-helix model of the polymer.[46,52] The Gaussian broadening of the calculated spectra was performed with the reported experimental[5] energy resolution of 1.3 eV.

The calculated and the experimentally measured[5] XRS spectra for aligned polyfluorene with different momentum transfer values is presented in Fig. 3. The agreement between the calculation and the experiment is very good. In the upper curves the most notable difference is the nonexistence of the peak at 285 eV in the calculated spectrum when **q** is along the drawing axis of the polymer. This peak is a signature of the π-type bonding of the carbon atoms in the backbone of the polymer.[53] Its absence was observed also in the calculations made in Ref. 5, where this was interpreted as an indication of the misalignment of the polymers in the sample. This argument was justified using a complementary x-ray diffraction based analysis, which showed that the polymers had only partial orientation preference along the drawing axis, and that the order of misalignment comprehensively explained the feature. Other potential sources for the observation, such as quickly emerging defects caused by radiation damage, were concluded not to impede this interpretation. Our method also reproduces the experimental spectrum in the first few eVs above the edge with a good accuracy. In the lower curves there is likewise remarkable similarity between the calculated and the experimental spectra. The intensities of the calculated peaks at 285 eV agree with the experimental ones, although especially for $q = 5.13$ a.u. the peak is somewhat too broad. The shoulder in all experimental spectra at 288 eV is present in the calculated spectra at slightly lower energy, but also this feature is broadened too much. After an analysis of the localization of the final state orbitals, we associate the shoulder with the transitions to orbitals that have significant contribution between carbon and hydrogen atoms. This is consistent with Dhez *et al.*,[53] who studied the near-edge spectra of similar polymers and found out that the peaks in this region can often be related to C-H bonds.

B. Symmetry analysis of the unoccupied states

An important aspect of XRS is the high localization of the core hole (and thus also the high localization of the initial KS orbital). This allows the study of the electronic structure in the vicinity of the atoms of a specific element in the system. Together with the high symmetry of the core state this makes it also possible to extract the symmetry properties of the unoccupied states from the experimental XRS spectra. This was recently illustrated for MgB_2.[4]

In the framework of the recently proposed calculation scheme,[4,24] we have developed a method for performing the symmetry analysis of the unoccupied electronic states for molecular systems. To perform the analysis, the values of the transition matrix elements must be divided into different transition channels. For each transition $|i\rangle \rightarrow |f\rangle$, a matrix $M^{if}(\mathbf{q})$ can be constructed, whose element $M^{if}_{l_i l_f}(\mathbf{q})$ corresponds to the transition rate of the channel $l_i \rightarrow l_f$, where l_i and l_f are the angular momentum quantum numbers for the initial and the final states, respectively. The sum of the elements of $M^{if}(\mathbf{q})$ is equivalent to the value of the transition matrix element,

$$\sum_{l_i l_f} M^{if}_{l_i l_f}(\mathbf{q}) = \langle i | e^{i\mathbf{q}\cdot\mathbf{r}} | f \rangle. \tag{4}$$

We proceed by expressing the KS orbitals as linear combinations of *s*, *p*, *d*, etc. contributions around the excited atom,

corresponding to the angular momentum quantum number values $l=0,1,2$, etc., respectively:

$$\phi_n(\mathbf{r}) \approx \sum_{l=0}^{l_{max}} \sum_{m=-l}^{l} c_n^{lm}(r) Y_{lm}(\hat{\mathbf{r}}), \tag{5}$$

where $c_n^{lm}(r)$ are radial functions and $Y_{lm}(\hat{\mathbf{r}})$ spherical harmonics centered at the excited atom. The equation becomes exact if $l_{max}=\infty$. In this work we have used the truncation at $l_{max}=2$. The radial functions can be solved by spherical integration,

$$c_n^{lm}(r) = \int d\Omega \phi_n(\mathbf{r}) Y_{lm}^*(\hat{\mathbf{r}}). \tag{6}$$

Using the expression $\exp(i\mathbf{q}\cdot\mathbf{r})=4\pi\Sigma_{lm} i^l j_l(qr) Y_{lm}^*(\hat{\mathbf{q}}) Y_{lm}(\hat{\mathbf{r}})$, where $j_l(qr)$ is a spherical Bessel function, it follows from Eqs. (4) and (5) that

$$M_{l_i l_f}^{if}(\mathbf{q}) = 4\pi \sum_{m_i=-l_i}^{l_i} \sum_{m_f=-l_f}^{l_f} \sum_{l=0}^{l_i+l_f} \sum_{m=-l}^{l} i^l Y_{lm}^*(\hat{\mathbf{q}}) \times \int_0^\infty dr r^2 c_i^{l_i m_i *}(r) c_f^{l_f m_f}(r) j_l(qr) \times \int d\Omega Y_{l_i m_i}^*(\hat{\mathbf{r}}) Y_{l_f m_f}(\hat{\mathbf{r}}) Y_{lm}(\hat{\mathbf{r}}). \tag{7}$$

The radial integral can be calculated numerically and the angular integral using Gaunt's formula. The diagonal elements of the matrix product $N^{if}(\mathbf{q})=M^{if\dagger}(\mathbf{q})M^{if}(\mathbf{q})$ correspond to the desired transition rates to $s,p,d,\ldots$-type final states.

In general, the truncation of the sum over l in Eq. (5) at $l_{max}=2$ results in an incorrect form of the KS orbitals. This is especially true for the delocalized valence and unoccupied orbitals that do not possess the center of symmetry at the excited atomic site. However, the scheme can be justified for the case of inner-shell excitations. First, the high symmetry and localization of the initial orbital means that the correct form of this orbital is conserved to a high accuracy when using Eq. (5). Second, from the previous studies we know that even with moderately high values of q, the transitions from the $1s$ state to the states with $l>2$ do not give a significant contribution to the spectrum in the XANES region, and can thus be neglected.[24] Furthermore, Eq. (4) provides a quantitative scheme to validate the use of the truncation: After obtaining the contributions of the different channels, their sum can be compared with the value calculated using the Gaussian integral based method where the complete KS orbitals are included.

In Fig. 4 we illustrate the decomposition method for the aromatic molecules in the large momentum transfer region ($q=9.0$ a.u., spherical average). The XRS spectrum is decomposed into s-, p-, and d-type final state contributions. The peaks at around 285 eV originate completely from $s\rightarrow p$ transitions, and the local density of unoccupied states in this region is essentially equivalent to the p-type local density of states. These states are π^*-type antibonding states and their existence can be associated with the π-type bonding of the carbon atoms in aromatic molecules.[53] The transitions to s-type final states (monopole transitions) gain weight especially at 290–295 eV, while the contribution of the transitions to d-type final states is still very small in the energy transfer region studied here.

The transition channel decomposition was also calculated for the polyfluorene. The decompositions are shown in Fig. 5. In these calculations, the momentum transfer vector was perpendicular to the drawing axis of the polyfluorene. It can be seen that the peak at 285 eV is completely p-type, analogously to the case of aromatic molecules. This is in agreement with the picture of π-type bonding mentioned above. The small shift of the maximum of the spectrum at around 291 eV towards slightly higher energy is due to the $s\rightarrow s$ monopole transitions that gain weight when q becomes larger.

In Fig. 5 we present also the results of the validation test of our decomposition method. We compared the sum of the diagonal elements of $N^{if}(\mathbf{q})$ with the total transition rate ($|\langle f|e^{i\mathbf{q}\cdot\mathbf{r}}|i\rangle|^2$), which was calculated using the Gaussian integral based method. The difference between the spectra calculated in the two ways was found to be negligible. We also checked that the nondiagonal elements of $N^{if}(\mathbf{q})$ were very small. These observations justify the use of our approach in the present case. In general, this comparison should always be made.

Finally we discuss how the symmetry analysis of the electronic states enables the interpretation of the XRS spectra in terms of the bonding properties of the materials studied. In the case of hydrocarbon molecules, the strong prepeak at around 285 eV at low momentum transfer (Fig. 2) is a sign of π-type bonding between carbon atoms. The enhancement of the features at 287–290 eV with increasing momentum transfer (Fig. 4) is due to the presence of the σ-type bonds between carbon and hydrogen atoms. The σ bonds between the carbon atoms can be related to the features above 290 eV, which are also enhanced with higher momentum transfer. The changes between the low and high momentum transfer XRS spectra of polyfluorene (Fig. 3) are less clear, even though the bonding properties of the polyfluorene backbone are very similar to the hydrocarbon molecules. Here, however, the contribution of the side chains to the total spectrum partly overlays the contribution of the backbone, thus hindering the distinguishment of the specific features. Furthermore, the momentum transfer of 5.13 a.u. used in the case of polyfluorene may not be sufficiently large to enhance these features enough.

IV. CONCLUSIONS

We have developed a computational method for calculating double differential cross sections for the nonresonant x-ray Raman scattering from molecules and molecular systems. Our method is based on the density functional theory, and the orbital relaxation caused by the inner-shell excitation is included using transition potential approximation. We have successfully applied our scheme in analyzing the carbon K-edge XRS spectra of aromatic molecules and aligned

polyfluorene. The agreement between the calculations and the experimental results was very good. We also illustrated that our method can be used to decompose the spectrum into different transition channels, thus allowing the study of the symmetry properties of the unoccupied electronic states. This analysis can be applied to elucidate the bonding properties of the chemical systems of interest. As the use of x-ray Raman scattering is expected to increase and extend to new materials in the future, these features will be useful for interpreting the near-edge spectra of molecules, polymers, and other nanoscale structures.

ACKNOWLEDGMENTS

This work has been supported by the Research Funds of the University of Helsinki and the Academy of Finland through its Centers of Excellence program (2006-2011) and Contracts No. 1201291, No. 1205967, and No. 1110571.

[1] S. K. Sinha, J. Phys.: Condens. Matter **13**, 7511 (2001).
[2] U. Bergmann, P. Glatzel, and S. P. Cramer, Microchem. J. **71**, 221 (2002).
[3] A. Mattila, J. A. Soininen, S. Galambosi, S. Huotari, G. Vankó, N. D. Zhigadlo, J. Karpinski, and K. Hämäläinen, Phys. Rev. Lett. **94**, 247003 (2005).
[4] J. A. Soininen, A. Mattila, J. J. Rehr, S. Galambosi, and K. Hämäläinen, J. Phys.: Condens. Matter **18**, 7327 (2006).
[5] S. Galambosi, M. Knaapila, J. A. Soininen, K. Nygård, S. Huotari, F. Galbrecht, U. Scherf, A. P. Monkman, and K. Hämäläinen, Macromolecules **39**, 9261 (2006).
[6] T. Suzuki, J. Phys. Soc. Jpn. **22**, 1139 (1967).
[7] Y. Mizuno and Y. Ohmura, J. Phys. Soc. Jpn. **22**, 445 (1967).
[8] J. Stöhr, *NEXAFS Spectroscopy* (Springer-Verlag, Berlin, 1992).
[9] J. J. Rehr and R. C. Albers, Rev. Mod. Phys. **72**, 621 (2000).
[10] S. Doniach, P. M. Platzman, and J. T. Yue, Phys. Rev. B **4**, 3345 (1971).
[11] C. Sternemann, J. A. Soininen, S. Huotari, G. Vankó, M. Volmer, R. A. Secco, J. S. Tse, and M. Tolan, Phys. Rev. B **72**, 035104 (2005).
[12] Ph. Wernet, D. Nordlund, U. Bergmann, M. Cavalleri, M. Odelius, H. Ogasawara, L. Å. Näslund, T. K. Hirsch, L. Ojamäe, P. Glatzel, L. G. M. Pettersson, and A. Nilsson, Science **304**, 995 (2004).
[13] K. Hämäläinen, S. Galambosi, J. A. Soininen, E. L. Shirley, J.-P. Rueff, and A. Shukla, Phys. Rev. B **65**, 155111 (2002).
[14] J. A. Soininen, K. Hämäläinen, W. A. Caliebe, C.-C. Kao, and E. L. Shirley, J. Phys.: Condens. Matter **13**, 8039 (2001).
[15] Y. Meng, H.-K. Mao, P. J. Eng, T. P. Trainor, M. Newville, M. Y. Hu, C. Kao, J. Shu, D. Hausermann, and R. J. Hemley, Nat. Mater. **3**, 111 (2004).
[16] J. J. Ritsko, S. E. Schnatterly, and P. C. Gibbons, Phys. Rev. B **10**, 5017 (1974).
[17] N. Jiang and J. C. H. Spence, Phys. Rev. B **69**, 115112 (2004).
[18] M. Tomellini and P. Ascarelli, Solid State Commun. **72**, 371 (1989).
[19] D. E. Sayers, E. A. Stern, and F. W. Lytle, Phys. Rev. Lett. **27**, 1204 (1971).
[20] H. Wende, Rep. Prog. Phys. **67**, 2105 (2004).
[21] J. A. Soininen and E. L. Shirley, Phys. Rev. B **64**, 165112 (2001).
[22] E. L. Shirley, Phys. Rev. Lett. **80**, 794 (1998).
[23] M. Alagia, C. Baldacchini, M. G. Betti, F. Bussolotti, V. Carravetta, U. Ekström, C. Mariani, and S. Stranges, J. Chem. Phys. **122**, 124305 (2005).
[24] J. A. Soininen, A. L. Ankudinov, and J. J. Rehr, Phys. Rev. B **72**, 045136 (2005).
[25] L. Triguero, L. G. M. Pettersson, and H. Ågren, Phys. Rev. B **58**, 8097 (1998).
[26] T. Mizoguchi, I. Tanaka, M. Yoshiya, F. Oba, K. Ogasawara, and H. Adachi, Phys. Rev. B **61**, 2180 (2000).
[27] H. Ågren, V. Carravetta, L. G. M. Pettersson, and O. Vahtras, Phys. Rev. B **53**, 16074 (1996).
[28] J. C. Slater, Adv. Quantum Chem. **6**, 1 (1972).
[29] P. A. Lee and G. Beni, Phys. Rev. B **15**, 2862 (1977).
[30] G. Fronzoni and P. Decleva, Chem. Phys. **237**, 21 (1998).
[31] T. Tyliszczak, I. G. Eustatiu, A. P. Hitchcock, C. C. Turci, A. B. Rocha, and C. E. Bielschowsky, J. Electron Spectrosc. Relat. Phenom. **114**, 93 (2001).
[32] M. Stener, G. Fronzoni, and M. de Simone, Chem. Phys. Lett. **373**, 115 (2003).
[33] B. Moulton and M. J. Zaworotko, Chem. Rev. (Washington, D.C.) **101**, 1629 (2001).
[34] M. Grell, W. Knoll, D. Lupo, A. Meisel, T. Miteva, D. Neher, H.-G. Nothofer, U. Scherf, and A. Yasuda, Adv. Mater. (Weinheim, Ger.) **11**, 671 (1999).
[35] U. Scherf and E. J. W. List, Adv. Mater. (Weinheim, Ger.) **14**, 477 (2002).
[36] F. Galbrecht, X. H. Yang, B. S. Nehls, D. Neher, T. Farrell, and U. Scherf, Chem. Commun. (Cambridge) **18**, 2378 (2005).
[37] In this work we use Hartree atomic units $e=\hbar=m_e=1$, except for the figures where energies are given in eVs.
[38] P. Hohenberg and W. Kohn, Phys. Rev. **136**, B864 (1964).
[39] W. Kohn and L. J. Sham, Phys. Rev. **140**, A1133 (1965).
[40] R. O. Jones and O. Gunnarsson, Rev. Mod. Phys. **61**, 689 (1989).
[41] J. F. Janak, Phys. Rev. B **18**, 7165 (1978).
[42] K. Triguero, O. Plashkevych, H. Ågren, and L. G. M. Pettersson, J. Electron Spectrosc. Relat. Phenom. **104**, 195 (1999).
[43] O. Takahashi, K. Saito, M. Mitani, H. Yoshida, F. Tahara, T. Sunami, K. Waki, Y. Senba, A. Hiraya, and L. G. M. Pettersson, J. Electron Spectrosc. Relat. Phenom. **142**, 113 (2005).
[44] STOBE-DEMON version 2.1, K. Hermann, L. G. M. Pettersson, M. E. Casida, C. Daul, A. Goursot, A. Koester, E. Proynov, A. St-Amant, and D. R. Salahub, contributing authors: V. Carravetta, H. Duarte, C. Friedrich, N. Godbout, J. Guan, C. Jamorski, M. Leboeuf, M. Leetmaa, M. Nyberg, L. Pedocchi, F. Sim, L. Triguero, and A. Vela, StoBe Software, 2005.
[45] M. L. Gordon, D. Tulumello, G. Cooper, A. P. Hitchcock, P. Glatzel, O. C. Mullins, S. P. Cramer, and U. Bergmann, J. Phys. Chem. A **107**, 8512 (2003).
[46] M. Knaapila, K. Kisko, B. P. Lyons, R. Stepanyan, J. P. Foreman, O. H. Seeck, U. Vainio, L.-O. Pålsson, R. Serimaa, M. Torkkeli, and A. P. Monkman, J. Phys. Chem. B **108**, 10711 (2004).

[47] All basis sets are available at http://www.demon-software.com/public_html/download.html#basis
[48] B. Hammer, L. B. Hansen, and J. K. Nørskov, Phys. Rev. B **59**, 7413 (1999).
[49] J. P. Perdew, K. Burke, and M. Ernzerhof, Phys. Rev. Lett. **77**, 3865 (1996).
[50] S. Huzinaga, L. Seijo, Z. Barandiarán, and M. Klobukowski, J. Chem. Phys. **86**, 2132 (1987).
[51] The exact energy shifts for benzene, naphthalene, anthracene, triphenylene, and polyfluorene are 1.6, 1.7, 2.5, 1.3, and 1.7 eV, respectively.
[52] B. Tanto, S. Guha, C. M. Martin, U. Scherf, and M. J. Winokur, Macromolecules **37**, 9438 (2004).
[53] O. Dhez, H. Ade, and S. G. Urquhart, J. Electron Spectrosc. Relat. Phenom. **128**, 85 (2003).